Thermal diffusivity of the Mott insulator Ca_2RuO_4 in a non-equilibrium steady state

Shuji Kawasaki[1], Akitoshi Nakano[1], Hiroki Taniguchi[1], Hai Jun Cho[2], Hiromichi Ohta[2], Fumihiko Nakamura[3] and Ichiro Terasaki[1]

[1]*Department of Physics, Nagoya University, Nagoya 464-8602, Japan*
[2] *Research Institute for Electronic Science, Hokkaido University, Sapporo 001-0020, Japan*
[3] *Department of Education and Creation Engineering, Kurume Institute of Technology, Kurume 830-0052, Japan*

We have measured and analyzed the in-plane thermal diffusivity of the Mott insulator Ca_2RuO_4 around room temperature under external currents with an infrared camera as a contactless thermometer. We find that the thermal diffusivity decreases by 40 % for an external current density of 14 A/cm^2. This large impact on lattice properties highly nontrivial in the sense that the external current primarily affects the electronic states. A possible explanation for this is disucussed.

A great success in statistical physics has revealed the relationship of thermodynamic variables to microscopic parameters for individual materials, and has explained the universality and diversity of condensed matter physics. To expand its applicability towards non-equilibrium states, the non-equilibrium steady state (NESS) has been long investigated. NESS is a system characterized by steady flows of energy and particle, where thermodynamics is expected to partially remain valid.[1,2] An electrical conductor subjected to an external constant current offers a prime example of NESS,[3] and we have studied NESS in non-ohmic conductors.[4–6]

Among non-ohmic conductors, the Mott insulator Ca_2RuO_4 has occupied a unique position. Ca_2RuO_4 crystallizes in the K_2NiF_4 type structure, where the conductive RuO_2 planes consisting of the corner-shared RuO_6 octahedra are stacked with the CaO double layer along the c axis. Nakatsuji et al.[7] first synthesized this oxide, and later Alexander et al.[8] found a first-order metal-insulator transition around 360 K. We have studied external-current dependence of physical properties in Ca_2RuO_4,[9–14] since Nakamura et al.[15] discovered a giant nonlinear conduction at room temperature. Okazaki et al.[9] established a measurement technique of nonlinear conduction using infrared thermometer, and successfully separated the intrinsic nonlinear conduction from artifacts due to self-heating.[16] Nishina et al.[11] observed the Seebeck coefficient enhanced by a constant current flow. Very recently, Terasaki et al.[14] found that a time scale of the non-linear conduction is of the order of 10^{-2} sec, implying that the lattice subsystem needs to be relaxed against the external current. This further suggests that the electron subsystem strongly affects the lattice subsystem through the strong electron-lattice coupling in this layered ruthenate.[17,18] The external current also affects the lattice system through the Mott gap suppression.[13,19–21]

Thermal conductivity κ and thermal diffusivity D is yet another transport parameter, and is expected to be affected by external currents. These quantities work as the last missing link in NESS, in the sense that ρ, S and κ comprehensively describe the Boltzmann equation in the absence of magnetic fields. Here we report how the thermal transport is modified under an electrical current flow. We have established the measurement and analysis technique of thermal diffusivity under electrical currents, and found that the in-plane thermal diffusivity of Ca_2RuO_4 decreases by 40 % for a current density of 14 A/cm^2.

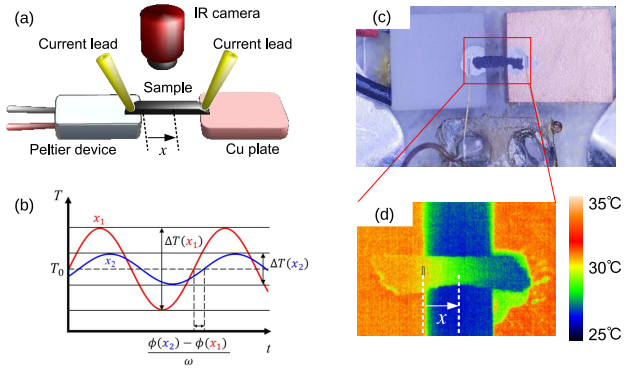

Fig. 1. (Color online) (a) Schematic of the measurement setup. The sample bridges the Peltier device and the copper plate, and is connected to the current leads. Temperature distribution at x is monitored by the infrared camera. (b) Schematic of the time-dependent temperature at different points x_1 and x_2. (c) Photographic image of the sample mount. (d) Thermal image around the sample.

Single-crystal samples of Ca_2RuO_4 were grown by a floating-zone method. The detailed conditions and characterization were given elsewhere.[22]

Cross-plane thermal diffusivity was measured at room temperature by the time domain thermoreflectance (PicoTR, PicoTherm Co.)[23] The 100-nm-thick Mo was deposited on the sample as a transducer by dc sputtering. The results were simulated using the packaged software.

In-plane thermal diffusivity was measured with a home-made measurement station based on an ac-calorimetric method.[24] The experimental setup is schematically shown in Fig. 1(a). The sample bridged the Peltier device (Lasercreate TES1-0401BT125S) and the copper plate with silver paint (Dupont 4922N). The gold wires were attached as current leads to supply external current. The top-surface temperature (the temperature between the voltage pads at the top surface of the sample) was monitored with an infrared thermal image camera with a spatial resolution of 5.3×5.3 μm^2 (Vision Sensing, VIM-640G2ULC) and a time resolution of 33 ms. The temperature resolution was 50 mK at room temperature. A typical photographic image of the sample mount is shown

in Fig.1(c). Figure 1(d) shows a photographic image around the sample with a dimension of 2.1×0.46×0.13 mm^3.

Let us start from the measurement principle of the ac calorimetric method. As schematically shown in Fig. 1(b), an sinusoidal heating/cooling is given by the Peltier device, and the generated heat wave propagates through the sample, causing the corresponding local temperature wave of $T(x,t)$ at position x from the edge of the device at time t. Suppose $x_1 < x_2$, then the amplitude of the local temperature should be larger at x_1 than at x_2. Likewise the phase delay is smaller at x_1 than at x_2.

We find the analytical expression of $T(x,t)$ based on a conventional theory of heat conduction. The heat balance equation at T is generally given by $\partial q/\partial t + \nabla\cdot(\kappa\nabla(-T)) = q_{\rm ext}$, where q is the heat density in the sample and $q_{\rm ext}$ is the external heat density supplied to the sample. Assuming one-dimensional conduction in the experimental configuration shown in Fig. 1(a), we rewrite the heat balance equation with respect to $T = T(x,t)$ as

$$c\frac{\partial T}{\partial t} + \frac{2\delta}{d}(T - T_b) - \kappa\frac{\partial^2 T}{\partial x^2} = \frac{Q_0 e^{i\omega t}}{d}, \qquad (1)$$

where c is the specific heat per volume of the sample. The second term in the left hand side represents the thermal conduction to the heat bath, where δ is the heat conductance per unit area between the Peltier device and the bottom of the sample, d the sample thickness, and T_b the temperature at the surface of the Peltier device. The right hand side represents the external heat flux, where $Q_0 e^{i\omega t}$ is the ac heat flux per unit area from the Peltier device to the sample.

A wave-form solution for Eq. (1) is given by $T(x,t) = \Delta T e^{i(\omega t-\phi)} + T_b$, and the amplitude and phase are given by

$$\Delta T = \frac{Q_0}{2\omega c d\sqrt{1+(\omega\tau)^2}} e^{-k_a x} \qquad (2)$$

$$\phi = k_p x + \phi_0, \qquad (3)$$

where k_a and k_p can be obtained from the amplitude and phase of the observed temperature oscillation as

$$k_a = -\frac{d\ln(\Delta T)}{dx} \qquad (4)$$

$$k_p = \frac{d\phi}{dx} \qquad (5)$$

Using the experimentally-obtained k_a and k_p, frequency-dependent thermal diffusivities D_a and D_p for the amplitude and phase parts are calculated as $D_i = \omega/2k_i^2$ ($i = a$ and p), and the thermal diffusivity D is finally obtained as

$$D = \sqrt{D_a D_p}. \qquad (6)$$

Figure 2(a) shows $T(x,t)$ for $x = 0.15$ and 0.56 mm for 0.10 Hz. The temperature changes sinusoidally and the amplitude is larger at 0.15 mm, and the phase delay is larger at 0.56 mm. Figure 2(b) shows $T(x,t)$ for 0.30 Hz. The x dependence is similar to that in Fig. 2(a), but the amplitude is smaller than at 0.1 Hz. By fitting $T(x,t)$ with a sinusoidal wave, the amplitude ΔT and the phase $\phi-\phi_0$ were determined at various x and various frequencies $f = \omega/2\pi$. Thus obtained ΔT and $\phi - \phi_0$ are plotted as a function of x in Figs. 2 (c) and (d), respectively. The dotted lines in the figures represent linear fitting, from the slope of which k_a and k_p are determined through Eqs. (4)(5).

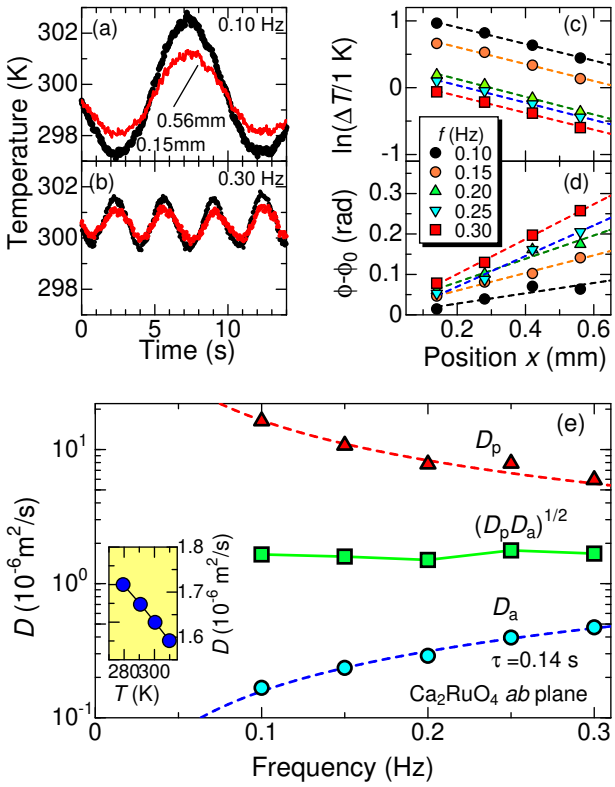

Fig. 2. (Color online) Time-dependent temperature at two points of the distance from the edge of the Peltier device $x = 0.15$ and 0.56 mm for an ac- heat frequency of (a) 0.1 Hz and (b) 0.30 Hz. (c) The amplitude and (d) phase of the temperature oscillation plotted as a function of the position from the edge of the Peltier device. (e) The in-plane thermal diffusivities D_a and D_p obtained from the data shown in (c) and (d) plotted as a function of frequency. The dotted curves are theoretical fitting with a time constant of 0.14 s. The inset shows the temperature dependence of the in-plane thermal diffusivity of Ca_2RuO_4.

The obtained D_a and D_p from k_a and k_p are shown as a function of frequency in Fig. 2(e). The dotted curves are theoretically predicted frequency dependence given by

$$D_a = D\left[\sqrt{(p+1)/2} + \sqrt{(p-1)/2}\right]^{-2} \qquad (7)$$

$$D_p = D\left[\sqrt{(p+1)/2} - \sqrt{(p-1)/2}\right]^{-2}, \qquad (8)$$

where $p = \sqrt{1+(1/\omega\tau)^2}$ with $\tau = 0.14$ s. The experimental data and the theoretical curves are consistent, and the thermal diffusivity $D = \sqrt{D_a D_p}$ is determined to be 1.64×10^{-6} m^2/s, being essentially independent of frequency as shown by the open squares. Throughout the experiment, we assumed the one-dimensional heat conduction, where the sample temperature is expected to be constant along the thickness direction. To see this, we evaluate the thermal diffusion length to be $\sqrt{2D/\omega} = 2.3$ mm for 0.1 Hz. This value is found to be one-order-of-magnitude larger than the sample thickness of 0.13 mm, satisfying the condition of the one-dimensional heat conduction.

The obtained thermal diffusivity is close to that of high-temperature superconducting copper oxides,[25] and much smaller than that of insulating perovskite oxides.[26] As is generally agreed, most oxides are good heat conductors, for an oxygen ion is a light element tightly bound via ionic bonding

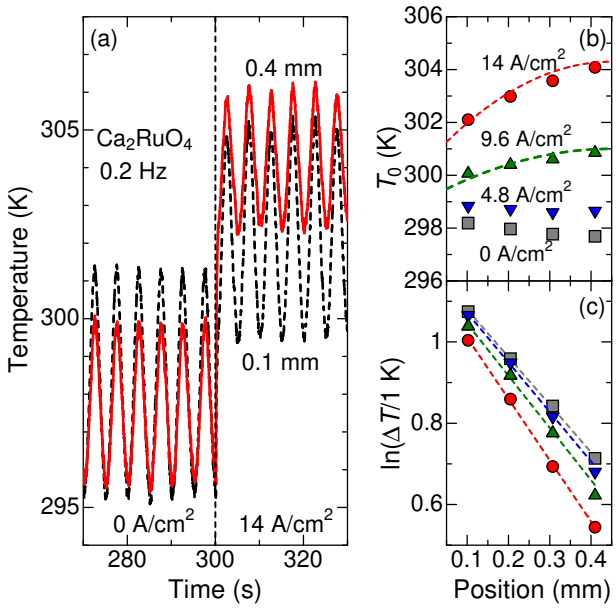

Fig. 3. (Color online) (a) Time-dependent temperature with and without a current density of 14 A/cm^2. The external current is applied at 300 s. (b) Local average temperature T_0 plotted as a function of x. The two dotted curves represent the Joule heating effects given by Eq. 9 (see text). (c) Temperature oscillation plotted as a function of the position from the edge of the Peltier device x. The dotted lines represent the linear fitting.

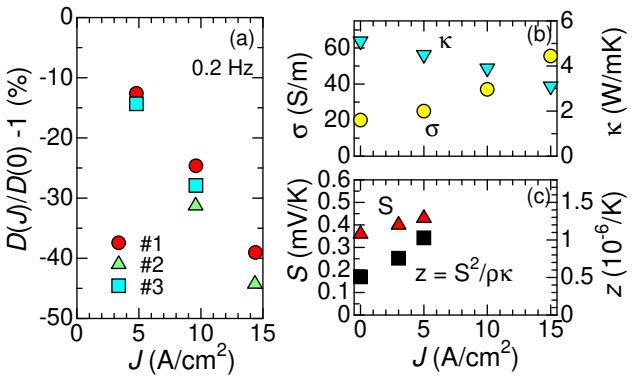

Fig. 4. (Color online) (a) Relative change in the thermal diffusivity plotted as a function of current density J. (b) Electrical σ and thermal κ conductivities, (c) the Seebeck coefficient S and the figure of merit z plotted as a function of current density J.

in oxides; Sapphire and ZnO are typical examples. In contrast, strongly-correlated oxides tend to show a lower thermal diffusivity partly owing to the strong electron-lattice coupling.

Using a bulk density ρ_g of 4.5×10^3 kg/m^3 and a specific heat c_g of 6.9×10^2 J/kgK,[27] the in-plane thermal conductivity is evaluated to be $\kappa_{\parallel} = D\rho_g c_g = 5.1$ W/mK. On the other hand, the cross-plane thermal conductivity $\kappa_{\perp}$ was evaluated to be 1.8 W/mK, and the anisotropy ratio R_κ (= $\kappa_{\parallel}/\kappa_{\perp}$) is determined to be 2.8 in this layered oxide. This value of R_κ is large in comparison with other anisotropic materials. In spite of the layered structures, the nature-made stones (igneous rocks) show smaller $R_\kappa \sim 1.5$.[28] Even if spring constants connecting neighbouring atoms are anisotropic, the atoms oscillate three-dimensionally in a collective way. For the related oxides, the thermal conductivity of the isostructural $(La,Eu)_2CuO_4$ shows a larger anisotropic ratio (~ 6),[29,30] but in this oxide magnetic excitation contributes much to the in-plane thermal conduction. Through partial substitution of Sr for La, holes are introduced to suppress magnetic excitation, and consequently, R_κ reduced to 2–2.5. The elastic constants are similar among La_2CuO_4,[31] Sr_2RuO_4,[32] and Ca_2RuO_4.,[33] and accordingly the anisotropy of the sound velocity and the thermal conductivity is also similar among the three compounds. In the case of materials consisting of Van-der-Waals bonds, a larger R_κ is reported in $Bi_{1.6}Pb_{0.4}Sr_2Co_2O_8$ (~ 6)[34] and $ZrTe_5$ (~ 12).[35]

Now we show the thermal transport under external current. Figure 3 (a) shows a typical temperature oscillation $T(x,t)$ with and without external current at 0.2 Hz. For 0 A/cm^2 (time $t < 300$ s), the position dependence of $T(x,t)$ is similar to that in Figs. 2 (a) and (b); ΔT is larger for smaller x. For a current density J of 14 A/cm^2 ($t > 300$ s), the average temperature T_0 at 0.1 mm increases by 4 K owing to the self-heating by the Joule heat, and the amplitude ΔT slightly decreases in comparison with ΔT for 0 A/cm^2. One can see clear change in ΔT induced by external current at $x = 0.4$ mm. First, T_0 increases from that at x =0.1 mm. This means that the sample temperature changes with x under external current. Second, ΔT at 0.4 mm is much smaller for 14 A/cm^2 than for 0 A/cm^2. This indicates k_a increases with external current, which is truly unexpected in the sense that the external current preliminary modifies the electron subsystem, while the thermal diffusivity is determined by the lattice subsystem. Third, the temperature oscillation is distorted from a sinusoidal wave for 14 A/cm^2; the signal is noisier, and the maximum and minimum temperatures seem to rock with a longer period. Owing to this distortion, the phase of the signal was ill-determined. We have finally discarded the information on the phase, and evaluate the relative change in D only from the information on the amplitude of ΔT.

Figure 3(b) shows T_0 as a function of position for various J. As mentioned above, the temperature is not homogeneous in the presence of current density. In the one-dimensional model we have assumed, the heat balance equation is given by $\mathrm{div}(\kappa(-\partial T/\partial x)) = \rho J^2$. Thus the temperature distribution due to the steady Joule heating is

$$T(x) = T(x_{\mathrm{mid}}) - \frac{\rho J^2}{2\kappa}(x - x_{\mathrm{mid}})^2, \qquad (9)$$

where x_{mid} is the center position of the sample. The two dotted curves represent the temperature distribution expected from Eq. (9). With $\kappa = 5.1$ W/mK and $x_{\mathrm{mid}} = 0.45$ mm, Equation (9) explains the observed $T(x)$ reasonably, where ρ is determined as a fitting parameter to be 1.2 and 0.95 Ω cm for J = 9.6 and 14 A/cm^2, respectively. If we take J dependence of κ into account (see below), ρ is determined to be 0.90 and 0.57 Ωcm for 9.6 and 14 A/cm^2, respectively. Although we did not measure ρ simultaneously in this experiment, but the estimated ρ reasonably agrees with previous experiments,[9,14] and can see non-ohmic behaviour against J.

Figure 3(d) shows ΔT as a function of position for various J. As already mentioned, ΔT decreases as a function of x remarkably for J = 14 A/cm^2. One can see the slope of $\ln(\Delta T/1\ \mathrm{K})$ against x increases with J in magnitude. This indicates a substantial increase in k_a and consequently, a substantial decrease in D with J.

Figure 4(a) shows the relative change in the thermal diffusivity plotted as a function of current density J for three sam-

ples (#1 corresponds to the data in Fig. 3). The obtained data are more or less consistent, and the thermal diffusivity linearly decreases with J, and reaches a 40% reduction for J = 14 A/cm^2. Since Ca_2RuO_4 is a Mott insulator, the thermal conduction is determined by acoustic phonons. Thus the present results clearly indicate that *the electrical current severely suppresses the lattice thermal conduction*. This is consistent with our previous report that the nonlinear conduction of this oxide is observed in a steady state of heat flow.[14)]

Let us discuss the current-dependent thermal diffusivity more quantitatively. Within a simplest model (Drude model), D can be written as $D = v\ell/3$, where v and ℓ are the sound velocity and the phonon mean free path, respectively.[36)] From the recently-observed elastic constants of Ca_2RuO_4,[33)] the in-plane transverse sound velocity v is evaluated to be $C_{44}/\rho_g = 2.6\times10^3$ m/s. Putting $D = 1.6\times10^{-6}$ m$^2/s$, we get ℓ = 1.8 nm, which is as long as several unit-cell lengths. The 40%-reduced phonon mean free path is still as long as a few unit-cell lengths, which justifies the Drude picture. For a time scale, the relaxation time $\tau = \ell/v$ is evaluated to be 6.9×10^{-14} s, which is longer than the 300-K Planckian time $\tau_P = \hbar/k_BT = 2.5\times10^{-14}$ s that is believed to be a lower limit of the phonon relaxation time.[37)] This is reasonable because the Planckian time is important when the temperature is higher than the Debye temperature. In the title compound, the Debye temperature is expected to be similar to that of Sr_2RuO_4 (410–460 K).[32)] Thus the phonon modes are partially excited, and the relaxation time will depend on phonon modes.[38)]

According to Okazaki et al.,[9)] the external current suppresses the Mott gap to increase the carriers thermally excited above the gap. It will be thus natural to expect that additionally-excited carriers scatter phonons and further decrease ℓ, for Ca_2RuO_4 possesses a strong electron-phonon coupling stemming from the relationship of t_{2g} levels to the RuO_6 distortion.[18)] Another possibility is that the external current distorts the RuO_6 octahedra through the gap suppression.[13,19–21)] If the distortion is inhomogeneous, the distortion can also be a scattering center for phonons. In fact, the Mott gap in this oxide is small at the crack or imperfection,[10)] the inhomogeneous distortion by the external current likely occurs.

The three parameters of ρ, S and κ are not only fundamentally interesting, but also technologically important in thermoelectric energy conversion.[38)] Figures 4(b) and (c) show the three parameters and the figure of merit $z = S^2/\rho\kappa$ at room temperature as a function of J.[9,11)] We find the three parameters change with external current in order that z increases. Since z determines the energy conversion efficiency, we propose that non-equilibrium steady states in a Mott insulator can be an effective tool to improve thermoelectric performance.

In summary, we have measured and analysed the in-plane thermal diffusivity of a single-crystal sample of the Mott insulator Ca_2RuO_4 with and without external currents. We have established a measurement technique for thermal diffusivity with external current, and have found that the thermal diffusivity dramatically decreases with external current (40% for a current density of 14 A/cm^2). This indicates that the external current first affects the electron subsystem, and then modifies the lattice subsystem possibly through the strong electron-lattice coupling of this oxide. By combining with our previous works, we find that the steady state characterized by the external current improves the thermoelectric energy conversion in Ca_2RuO_4.

The authors would like thank R. Okazaki, Y. Maeno, S. Yonezawa, T. Yoshida, N. Kikugawa, T. Suzuki for close collaboration in Kakenhi Project. This study was supported by a Grant-in-Aid for Scientific Research (Kakenhi Nos. 17H06136, 19H05791). This work was performed under the Cooperative Research Program of "Network Joint Research Center for Materials and Devices" (Nos. 20181015, 20191026, 20201021).

*Corresponding author: Ichiro Terasaki (terra@nagoya-u.jp)

1) Y. Oono and M. Paniconi: Prog. Theo. Phys. Suppl. **130** (1998) 29.
2) S. Sasa and H. Tasaki: J. Stat. Phys. **125** (2006) 125.
3) N. Garnier and S. Ciliberto: Phys. Rev. E **71** (2005) 060101.
4) F. Sawano, I. Terasaki, H. Mori, T. Mori, M. Watanabe, N. Ikeda, Y. Nogami, and Y. Noda: Nature **437** (2005) 522.
5) F. Sawano, T. Suko, T. S. Inada, S. Tasaki, I. Terasaki, H. Mori, T. Mori, Y. Nogami, N. Ikeda, M. Watanabe, and Y. Noda: J. Phys. Soc. Jpn. **78** (2009) 024714.
6) Y. Nogami, N. Hanasaki, M. Watanabe, K. Yamamoto, T. Ito, N. Ikeda, H. Ohsumi, H. Toyokawa, Y. Noda, I. Terasaki, H. Mori, and T. Mori: J. Phys. Soc. Jpn. **79** (2010) 044606.
7) S. Nakatsuji, S. Ikeda, and Y. Maeno: J. Phys. Soc. Jpn. **66** (1997) 1868.
8) C. S. Alexander, G. Cao, V. Dobrosavljevic, S. McCall, J. E. Crow, E. Lochner, and R. P. Guertin: Phys. Rev. B **60** (1999) R8422.
9) R. Okazaki, Y. Nishina, Y. Yasui, F. Nakamura, T. Suzuki, and I. Terasaki: J. Phys. Soc. Jpn. **82** (2013) 103702.
10) R. Okazaki, Y. Ikemoto, T. Moriwaki, F. Nakamura, T. Suzuki, Y. Yasui, and I. Terasaki: J. Phys. Soc. Jpn. **83** (2014) 084701.
11) Y. Nishina, R. Okazaki, Y. Yasui, F. Nakamura, and I. Terasaki: J. Phys. Soc. Jpn. **86** (2017) 093707.
12) K. Tanabe, H. Taniguchi, F. Nakamura, and I. Terasaki: Appl. Phys. Express **10** (2017) 081801.
13) R. Okazaki, K. Kobayashi, R. Kumai, H. Nakao, Y. Murakami, F. Nakamura, H. Taniguchi, and I. Terasaki: J. Phys. Soc. Jpn. **89** (2020) 044710.
14) I. Terasaki, I. Sano, K. Toda, S. Kawasaki, A. Nakano, H. Taniguchi, H. J. Cho, H. Ohta, and F. Nakamura: J. Phys. Soc. Jpn. **89** (2020) 093707.
15) F. Nakamura, M. Sakaki, Y. Yamanaka, S. Tamaru, T. Suzuki, and Y. Maeno: Sci. Rep. **3** (2013) 2536.
16) G. Mattoni, S. Yonezawa, and Y. Maeno: Appl. Phys. Lett. **116** (2020) 172405.
17) M. Braden, G. André, S. Nakatsuji, and Y. Maeno: Phys. Rev. B **58** (1998) 847.
18) T. Mizokawa, L. H. Tjeng, G. A. Sawatzky, G. Ghiringhelli, O. Tjernberg, N. B. Brookes, H. Fukazawa, S. Nakatsuji, and Y. Maeno: Phys. Rev. Lett. **87** (2001) 077202.
19) J. Bertinshaw, N. Gurung, P. Jorba, H. Liu, M. Schmid, D. T. Mantadakis, M. Daghofer, M. Krautloher, A. Jain, G. H. Ryu, O. Fabelo, P. Hansmann, G. Khaliullin, C. Pfleiderer, B. Keimer, and B. J. Kim: Phys. Rev. Lett. **123** (2019) 137204.
20) C. Cirillo, V. Granata, G. Avallone, R. Fittipaldi, C. Attanasio, A. Avella, and A. Vecchione: Phys. Rev. B **100** (2019) 235142.
21) H. Zhao, B. Hu, F. Ye, C. Hoffmann, I. Kimchi, and G. Cao: Phys. Rev. B **100** (2019) 241104.
22) S. Nakatsuji and Y. Maeno: J. Solid State Chem. **156** (2001) 26 .
23) T. Baba: Jpn. J. Appl. Phys. **48** (2009) 05EB04.
24) I. Hatta, Y. Sasuga, R. Kato, and A. Maesono: Rev. Sci. Instrum. **56** (1985) 1643.
25) J. Zhang, E. M. Levenson-Falk, B. J. Ramshaw, D. A. Bonn, R. Liang, W. N. Hardy, S. A. Hartnoll, and A. Kapitulnik: Proc. Nat. Acad. Sci. **114** (2017) 5378.
26) A. M. Hofmeister: Journal of Applied Physics **107** (2010) 103532.
27) T. Eto, K. Akagi, E. Takashima, T. Noda, T. Suzuki, and F. Nakamura: Extended Abstract for the JPS Meeting **71.2** (2016) 2216.

28) M. G. Davis, D. S. Chapman, T. M. Van Wagoner, and P. A. Armstrong: J. Geophys. Res. **112** (2007).
29) Y. Nakamura, S. Uchida, T. Kimura, N. Motohira, K. Kishio, K. Kitazawa, T. Arima, and Y. Tokura: Phys. C **185-189** (1991) 1409.
30) C. Hess, B. Büchner, U. Ammerahl, and A. Revcolevschi: Phys. Rev. B **68** (2003) 184517.
31) J. L. Sarrao, D. Mandrus, A. Migliori, Z. Fisk, I. Tanaka, H. Kojima, P. C. Canfield, and P. D. Kodali: Phys. Rev. B **50** (1994) 13125.
32) J. Paglione, C. Lupien, W. A. MacFarlane, J. M. Perz, L. Taillefer, Z. Q. Mao, and Y. Maeno: Phys. Rev. B **65** (2002) 220506.
33) H. Uchiyama and I. Terasaki: SPring-8/SACLA Research Report **9** (2021) 32.
34) I. Terasaki, H. Tanaka, A. Satake, S. Okada, and T. Fujii: Phys. Rev. B **70** (2004) 214106.
35) J. Zhu, T. Feng, S. Mills, P. Wang, X. Wu, L. Zhang, S. T. Pantelides, X. Du, and X. Wang: ACS Appl. Mater. Interfaces **10** (2018) 40740.
36) N. W. Ashcroft and N. D. Mermin: *Solid State Physics* (Thomson Learning, 1976).
37) C. H. Mousatov and S. A. Hartnoll: Nature Phys. **16** (2020) 579.
38) I. Terasaki, Thermal Conductivity and Thermoelectric Power of Semiconductors, Reference Module in Materials Science and Materials Engineering. Elsevier, 2016.